RSC Advances

ROYAL SOCIETY OF CHEMISTRY

www.rsc.org/advances

Hybrid magnetic scaffolds of gelatin-siloxane incorporated with magnetite nanoparticles effective for bone tissue engineering

Khandma Dashnyam [a,b], Roman A Perez [a,b], Rajendra K Singh [a,b], Eun-Jung Lee [a,b], Hae-Won Kim [a,b,c]

[a] Institute of Tissue Regeneration Engineering (ITREN), Dankook University, Cheonan 330-714, South Korea

[b]Department of Nanobiomedical Science & BK21 PLUS NBM Global Research Center for Regenerative Medicine, Dankook University, Cheonan 330-714, South Korea

[c] Department of Biomaterials Science, School of Dentistry, Dankook University, Cheonan 330-714, South Korea

---

* Corresponding author: Prof. H.-W. Kim

E-mail) kimhw@dku.edu; Tel) +82 41 550 3081; Fax) +82 41 550 3085

For: **RSC Advances**

Abstract

Magnetism-induced applications of nanomaterials and scaffolds are currently gaining great interest for their potential applications in tissue repair and disease treatment. Here, we prepare novel magnetic scaffolds of gelatin-siloxane (GS) hybrids for bone repair and regeneration by incorporating magnetite nanoparticles (MNs). MNs were incorporated during the sol-gel process of the organic-inorganic hybrids, and highly porous scaffolds were achieved via the free-drying method. The MNs incorporated up to 3 wt% were shown to uniformly distribute within the GS matrix. The incorporated MNs significantly improved the mechanical properties of the scaffolds, including resistance to static load and dynamic storage modulus (from 100 kPa to 450 kPa). The scaffolds presented superparamagnetic behaviors, and the saturation magnetization increased with increasing MN content. The GS-MN scaffolds showed excellent bone-bioactivity, inducing apatite minerals rapidly in a body simulating medium. Rat mesenchymal stem cells cultured on the scaffolds spread better on the MN-incorporated magnetic scaffolds, and cell proliferation significantly improved on the magnetic scaffolds with respect to MN-free scaffolds. Osteogenic differentiation, as assessed by alkaline phosphatase activity of cells, was significantly higher in the magnetic scaffolds, and, furthermore, the cellular mineralization behavior also greatly improved with the incorporation of MNs. The results suggest that the MNs incorporated at small concentrations are effective in stimulating cell growth and osteogenic differentiation in the GS hybrid porous scaffolds, and thus the magnetic hybrid scaffolds may be useful for bone tissue engineering.

Keywords: Hybrid composites; Nanoparticles; Magnetic scaffolds; Bioactivity; Bone regeneration

1. Introduction

Scaffolds play important roles in tissue engineering significantly affecting the related cell responses and tissue reactions due to their tuned physical and chemical properties. For bone tissue engineering, nanocomposite and hybrid scaffolds made of organic and inorganic biomaterials are of special interest as they largely possess the mechanical and biological properties necessary for bone cell differentiation and bone formation [1]. Sol-gel processed hybrid scaffolds constructed using silica-based inorganic sources and natural polymers (including chitosan, gelatin and collagen) are promising matrices that can be used for bone regeneration. Hybrid scaffolds possess bone-bioactivity with the ability to induce acellular mineralization, favorable cell adhesion and growth, and possible osteogenic differentiation of cells [2-5]. Protein molecules, due to their mild sol-gel process conditions, have also been incorporated in order to exert additional therapeutic efficacy [2].

Here we utilize the sol-gel processed hybrid scaffolds made of gelatin-siloxane (GS). In particular, we aim to provide magnetic functionality to the hybrid scaffolds by incorporating magnetite nanoparticles (MNs), consequently producing magnetic scaffolds. In fact, magnetic scaffolds have recently been found to be fascinating biomaterials [6,7], because of the electromagnetic field they produce and the consequent physical interactions with biologic ingredients and cells. This electromagnetic field has been shown to positively affect cells, including the stimulation of cell proliferation and osteogenic differentiation [6]. Magnetic scaffolds have even been observed to increase angiogenesis, an early, necessary step for bone regeneration [6]. When static magnetism was applied to E. Coli, cell proliferation significantly increased [8]. Similarly, when a static magnetic field was applied to

osteoblastic cells, the bone related phenotype expressions were enhanced [9-12]. Positive effects have also been shown for neural cells, where the neurite outgrowth considerably increased in the presence of magnetic nanoparticles. While the significant effects of the magnetic fields and the magnetism-inducing materials on cellular responses have been reported, the exact mechanisms have yet to be elucidated. One plausible mechanism that has been proposed is that of magnetic-induced mechanotransduction and the consequent alteration of ion channels and intracellular signaling processes [13,14]

Here we produce novel magnetic scaffolds made of GS hybrid incorporating MNs. The MNs have been a fascinating nanomaterial in the medical field due to their excellent superparamagnetic properties [4,15,16]. We investigate the effects of the incorporation of MNs at small concentrations on the physico-chemical and mechanical properties of the hybrid scaffolds and on the cellular responses including proliferation and osteogenic differentiation.

2. Experimental Procedures

2.1. Preparation of Magnetite Nanoparticles

The magnetic nanoparticles (MNs) were prepared as described in our work elsewhere [7]. In brief, ferrous chloride tetrahydrate ($FeCl_2 \cdot 4H_2O$) in 1M HCl and ferric chloride hexahydrate ($FeCl_3 \cdot 6H_2O$) were mixed at room temperature (Fe^{2+}/Fe^{3+} = 1/2), and the resulting mixture was added drop-wise into 200 mL of 1.5M NaOH solution with vigorous stirring. After a short period of time, the resulting precipitate was then isolated by applying a magnetic field and then decanting the solution after centrifuging at 8000 rpm. The separation procedure was repeated twice, after which, 200 mL of 0.02 M HCl solution were added while continuously agitating. The product was again separated by centrifugation at 8000 rpm and dried at 40 °C. All steps were performed a nitrogen gas atmosphere to avoid oxidation.

2.2. Preparation of Magnetic Gelatin-Siloxane Scaffolds

The gelatin-siloxane (GS) scaffolds were prepared in almost the same manner that had been previously described in our work [13], with a slight modification to incorporate the MNs. Gelatin (type B, from bovine, Sigma), 3-(glycidoxypropyel) trimethoxysilane (GPTMS) (98%, Aldrich) and tetramethoxylsilane (TMOS) were used as reagents for the hybrid solution. Gelatin was dissolved in water at a concentration of 5 wt%. Separately, three different amounts of MNP were dispersed in DW: 1, 2 and 3 wt/wt %. These were then incorporated into gelatin solution, vortexed, and sonicated to achieve a homogenous dispersion of the nanoparticles in the gelatin solution. Afterwards, GPTMS and TMOS were added at a ratio of 10 wt% respect to gelatin with vigorous stirring for up to 3 h to produce the sol. Twenty microliters of HCl 1 M were added to the slurry to be used as the catalyst of the sol-gel reaction. The materials were left overnight to complete the gelation. The samples were then frozen for 3 h and lyophilized (Freeze-dryer, Ilshin lab Co., LTD) for 24 h to completely remove the water from the slurry and to produce the porous scaffold.

2.3. Characterization of Hybrid Scaffolds

The scaffolds were coated with gold and analyzed with SEM to observe the pore morphology as well as the surface morphology (SEM; JSM6330F, JEOL). The nanoparticle distribution in the gelatin matrix was analyzed via transmission electron microscopy (TEM; JEOL-7100). The porosity of the samples was measured by the amount of ethanol that was taken up. The chemical bond structure was investigated by using Fourier transform infrared spectroscopy (FT-IR; Perkin-Elmer). X-Ray diffraction was conducted to observe the crystallographic phases present (XRD, Philips MRD CuK_{α}, 40 kV, 20 mA).

2.4. Magnetic Properties of Hybrid Scaffolds

The initial magnetic response of the hybrid scaffolds was determined by measuring the minimum distance at which the scaffolds were attracted when a magnet was placed at a certain distance. The magnetic properties of the scaffolds were then studied under a magnetic field at room temperature by using a superconducting quantum interference device (SQUID, Quantum Design MPMS-XL7). Magnetic properties of the samples were evaluated in terms of the saturation magnetization and hysteresis loop area. Three samples were used for each condition (n = 3).

2.5. Water Uptake and Degradation of Scaffolds

A water uptake test was carried out by immersing the scaffolds into distilled water and measuring the weight change at 1, 3, 6, 12, and 24 h. The percentage of water uptake was calculated by using the following equation:

$$\Delta Wu\ (\%) = ((Ws-Wo)/Wo) \times 100,$$

where W_{ini} and W_{upt} are the sample weight before and after the water uptake test, respectively. Three samples were used for each condition (n = 3).

The degradation of the scaffolds was studied by placing them in phosphate buffer saline (PBS) at 37 ºC for up to 28 days. For each time interval, the samples were freeze-dried overnight, and the weight change was recorded. The percentage of degradation was calculated by using the following equation.

$$\Delta Wd\ (\%) = ((W_{ini}-W_{deg})/W_{ini}) \times 100,$$

where W_{ini} and W_{deg} are the recorded values before and after the degradation, respectively. Three samples were used for each condition (n = 3).

2.6. Mechanical Properties

The mechanical properties of the scaffolds were initially characterized through static stress measurements on wet scaffolds. A compression load was applied to a cylindrical sample (12 mm diameter x 6 mm thickness). The ability to resist deformation was recorded against time. Each measurement was performed on four samples, and the obtained values were averaged (n = 4).

Next, dynamic mechanical analysis (DMA; MetraVib, DMA25N) of the scaffolds was performed on a parallel plate configuration. Mechanical spectrometry was carried out by using a dynamic frequency sweep with frequencies ranging from 0.1–10 Hz at 37 °C with strain amplitude of 5%, which was within the linear range of the viscoelasticity. Both auto-tension and auto-strain adjustments were applied. Force was ramped from 0.001–0.2 N, and the maximum allowed strain was set to 10%. The storage modulus (E′) and loss modulus (E″) of the samples were measured. Tangent delta was calculated by the ratio of E″/ E′.

2.7. In Vitro Apatite-forming Ability

The *in vitro* apatite-forming ability of the scaffolds was considered in order to assess the acellular bone-bioactivity of the hybrid scaffolds. Samples were soaked in 1.5 times that of stimulated body fluid (1.5xSBF), which was generally used to accelerate the apatite-forming reaction and thus to shorten the period of observation for different time intervals of up to 14 days at 37 °C. At each time interval, samples were taken out, gently washed with distilled water several times, and freeze-dried. The weight change of the scaffolds during immersion was recorded, and apatite formation was observed via SEM, XRD, and FT-IR.

2.8. Cell Proliferation Assay

Mesenchymal stem cells (MSCs) derived from rat bone marrow were harvested from the femora and tibiae of adult rats (180–200 g) according to guidelines approved by the Animal Ethics Committee of Dankook University [17,18]. The harvested product was then centrifuged, and the supernatant was

collected and suspended within a culture flask containing normal culture medium which was composed of α-minimal essential medium (α-MEM) supplemented with 10% fetal bovine serum (FBS), 100 U/ml penicillin, and 100 mg/ml streptomycin in a humidified atmosphere of 5% CO_2 with air at a temperature of 37°C. After incubation for 1 day, the medium was refreshed and cultured until the cells reached near confluence. After the subculture was obtained and the cells were maintained in normal culture conditions, cells at 2–3 passages were used for further tests.

Scaffolds for cell tests were prepared with a dimension of 12 mm diameter x 6 mm thickness, which were sterilized in 70% ethanol overnight, rinsed three times with PBS and then placed in each well of 24-well plates.

Cell proliferation was evaluated at 7 and 14 days by using the double strained DNA assay kit. For this, the cell-cultured samples were washed twice with PBS and treated through freeze-thawing processes (2x) in order to achieve cell lysis. The cell lysates were centrifuged at 1500 rpm for 10 min to remove cell debris. The quantity of DNA present was determined spectrophotometrically with a commercially available dsDNA kit (Roche, Germany) in a microplate reader (Power WaveX, Bio-Tek Instruments, USA; 490 nm). A calibration curve with a decreasing concentration of cells was created to express the results of the cell number. The experiment was performed in triplicate.

2.9. Osteogenic Differentiation of Cells

Alkaline phosphatase (ALP) activity of cells was determined as it is considered as the osteogenic differentiation marker relatively at an early stage. After culture of cells had been kept in the osteogenic media for 7 and 14 days, samples were rinsed twice with PBS and treated with 1 mL of 0.2% Triton® X-100. Each sample was transferred into a 1.5 mL tube and was frozen for 1 h at -20 °C and thawed for 30 min at 4 °C. Following that the samples were centrifuged at 15,000 rpm for 20 min at 4 °C. Finally, the solution was analyzed for ALP. The supernatant was then transferred to a fresh 1.5 mL tube into which a 1:1:1 ratio of 1.5 M 2-amino-2-methyl-1-propanol (Sigma A58888), 1 mM $MgCl_2$, and 20 mM p-nitrophenyl phosphate (SigmaP4744) was added. After 3 h of incubation at 37 °C the reaction was terminated by adding 100 µL of 1 N NaOH. Optical density was measured at 405 nm

with a micro plate reader by using *p*-nitrophenol as a standard. The experiment was performed in triplicate.

2.10. Cellular Mineralization

The mineralization of cells on the hybrid scaffold was determined by using Alizarin Red S (ARS) staining (Sigma Aldrich). Cells were washed with PBS and fixed with 4% paraformaldehyde (PFA) for 10 min. After washing, samples were incubated in 2% w/v ARS solution (pH 4.1–4.3) in distilled water for 10 min at room temperature. The staining solution was removed, and the scaffolds were completely washed with distilled water. The stained samples were visualized by using a digital camera. For quantification of the mineralization, samples were incubated in 10% w/v cetylpyridinium chloride (CPC) in 10 mM sodium phosphate solution (pH 7) for 1 h, the reaction product was eluted, and the absorbance was measured at 595 nm using a microplate reader. The experiment was performed in triplicate.

2.11. Cell Morphology Observation

Cell morphology was also observed at each culture period (7, 14, and 21 days) by SEM. Samples prepared for SEM were initially washed in phosphate buffer 0.1 M at a pH of 7.4, fixed with a 2.5% glutaraldehyde (Sigma-Aldrich G400-4) solution in PBS, and were washed and maintained in 0.1 M phosphate buffer. Different ethanol solutions (50, 70, 90, 96, and 100% ethanol) were used to dehydrate the samples. Finally, hexamethyldisiliazane (HDMS, Fluka 52620) was used for complete dehydration, and platinum was used for coating for electron observation.

2.12. Statistical Analysis

The data are expressed as mean ± standard deviation, and statistical analysis was carried out by using a one way analysis of variance (ANOVA) followed by a Fisher post-hoc test. Statistical significance was considered at $p < 0.05$.

3. Results and Discussion

3.1. Physico-chemical, Magnetic and Mechanical Properties

The typical porous morphology of the hybrid scaffolds with varying MNs contents was observed via SEM (**Fig. 1a)**. All the scaffolds showed highly interconnected macroporous morphology, and the pore distribution was uniform. The distribution of the NMs within the GS matrix was examined via TEM (**Fig. 1b**). A TEM image of the scaffold (3%; the highest content of MNs) showed the distribution of nanoparticles with ~10 nm in size within the matrix, and the distributed nanoparticles were homogeneously observed throughout. An enlarged image showed the nanoparticles more clearly (black dots) which were mostly separated without being agglomerated. This implies there is well-dispersion of the MNs within the GS solution and homogeneous distribution of MNs within the hybrid scaffolds of at least up to 3% of MNs. In fact, the freeze-dried porous scaffolds incorporating MNs up to 3% showed to be well-shaped with a relatively uniform distribution of macropores, which, however, was severely hampered with the incorporation of MNs above 3%. Therefore, this content of MNs is considered to be the optimal condition for the production of GS-MNs nanocomposite scaffolds. It is known that the as-prepared MNs have relatively weak surface charge and thereby a weak electrostatic repulsion force. Therefore, the surface was coated with polymers or silica to enable homogeneous dispersion [7]. However, in the GS hybrid solution, the bare MNs were observed to achieve a stable emulsion state, which was considered to be due to the surface interactions with gelatin and/or siloxane. In other words, those media, with their negative charge properties, could facilitate an increase in the electrical repulsion of the MNs.

The phases of the produced hybrid scaffolds, as analyzed via XRD, showed the characteristic peaks of MNs with their incorporation (**Fig. 1c**). The FTIR spectrum showed the MNs bands (Fe-O at 560-600 cm^{-1}) along with the GS hybrid bands in the MNs-incorporated hybrids [7,9]. As the amount of

nanoparticles in the scaffolds increased, this peak intensity also increased. The three main peaks of the gelatin-related bands were also observed clearly; the C-N stretching mode for amide III at 1250 cm^{-1}, C=O stretching for amide I at 1690 cm^{-1}, and N-H deformation of amide II at 1560 cm^{-1} [19,20]. The siloxane-related bands, developed primarily due to the hydrolysis and polycondensation reactions, were also clearly shown, including the Si-O-Si asymmetric stretching vibration at 1093 cm^{-1}, symmetric stretching of Si-O-Si at 798 cm^{-1}, Si-OH stretching at 962 cm^{-1}, and OH stretching vibration at 3400 cm^{-1}. The results indicate that MNs-incorporated GS scaffolds were produced to have a typical form of siloxane-derived organic-inorganic hybrids.

The magnetic properties of the produced hybrid scaffolds were examined. Initially, the scaffolds were shown to be susceptible to an external static magnetic field. This was well demonstrated by measuring the minimum distance at which the magnet could attract the scaffold (**Fig. 2a**). The distance increased quite linearly with increasing MNs content; 0.2 cm for 0.5% MNs increased to 1 cm for 4% MNs, which implied that the magnetic properties could be tunable by altering the content of MNs. The magnetization of the scaffolds was more carefully examined by performing SQUID magnetometry. **Fig. 2b-c** shows the magnetization with respect to the magnetic field applied at a large (-20 kOe to +20 kOe) and a small range (-100 Oe to +100 kOe). While the pure GS scaffold showed little magnetization, the GS-MNs scaffolds showed a rapid increase in magnetization with a small magnetic field that was saturated quickly, and the behavior was extremely reversible with little energy loss. The magnetization behavior was typical of pure MNs, i.e., it was a superparamagnetic behavior [7]. The saturation magnetization of the magnetic scaffolds increased with increasing MNs content, from 0.24 emu/g for 1% MNs to 0.64 emu/g for 3% MNs (**Fig. 2d**). While the saturation magnetization value of the scaffolds was very small when compared to that of pure MNs (as high as 70 emu/g), the magnetization level was also considered to be effective for use in therapeutic scaffolds, such as that in bone cancer treatment, by generating magnetism-induced heat and stimulating bone tissue repair through magnetism-induced bone cell stimulation [6,10,14]

Since the magnetic hybrid scaffolds are used for tissue repair purpose, water-associated properties, including water uptake, swelling, and degradation are of special importance. Prior to the evaluations of water-associated properties of the scaffolds, we first assessed the porosity levels by means of ethanol-uptake method [2]. The ethanol uptake (in volume %) is meant to be the porosity of the

scaffolds. All the scaffolds showed similar levels of approximately 84-85%, implying the porosity levels were comparable for all scaffold compositions (**Fig. 3a**). Next we observed the water uptake capacity of the scaffolds (**Fig. 3b)**. For all compositions, water uptake occurred quickly within 1 h and increased slowly thereafter. The water uptake level increased as the MNs content increased, from ~350% for 0% MNs to ~550% for 3% MNs. The swelling degree of the scaffold in water also increased as the MNs content increased (**Fig. 3c)**, from ~11% for 0% MNs to ~17% for 3% MNs, indicating that the MNs-incorporated scaffolds showed higher volumetric increases in water. It is thus considered that the higher water uptake capacity of the MNs-incorporated scaffolds is primarily due to the increased volume of the scaffold since the porosity levels of scaffolds are in a similar range. It is intriguing that the MNs dispersed in the GS hybrid contribute to the dimensional extension of the matrix. The impregnated MNs, with their high hydrophilicity and negative-charged property, are thought to easily take up water molecules, which may possibly result in increasing the electrostatic repulsion between MN-MN and/or MN-matrix molecules.

The degradation behavior of the scaffolds was examined along with the swelling and water uptake properties (**Fig. 3c).** Degradation in PBS increased with time for all scaffolds where the 5-15% degradation seen after 7 days increased to 35-55% at 28 days. Moreover, the MNs-incorporation did not increase the degradation, but rather, the 0%-MNs scaffold showed the highest degradation (0% > 2% & 3% > 0%). It was generally expected that increased swelling and water uptake would lead to acceleration of degradation. Therefore, it is important to note that the reduced degradation of MNs-incorporated scaffolds was observed. Although MNs play a role in taking up a higher quantity of water molecules and lead to an increased dimensional change, the hybrid networks are considered to be stable without being disintegrated via a hydrolytic cleavage. It should also be noted that the in vitro degradation rates of our scaffolds observed herein were fairly comparable to those reported previously, where the scaffolds have similar natural polymer-silica hybrid compositions while showing excellent in vitro and in vivo tissue compatibility [2-5,13]. Furthermore, with regard to the possible degradation products, i.e., amino acids, silicon-based ionic groups, and iron ions, which resulting from gelatin, silica networks, and small amounts of MNs, respectively, previous studies on using either gelatin-silica materials or MNs-incorporating scaffolds have already shown favorable in vivo tissue compatibility [8-10]. Therefore, when deduced from these previous works, the current magnetic hybrid

scaffolds are expected to exert possibly acceptable biocompatibility, although more in-depth in vivo studies are needed in the future.

The mechanical properties of the hybrid scaffolds were subsequently analyzed in wet condition. Initially, a static compression test was performed using a constant force applied onto the scaffold while the induced strain was recorded with respect to time. Scaffolds showed a rapid initial increase in strain and then almost a plateau. Increase in MN content decreased the strain of the scaffolds, which was indicative of a higher resistance to deformation under a constant applied force **(Figs. 4a & b)**. Strain was reduced by as much as 5 times with 3%-MNs-incorporated scaffolds compared to that of the MNs-free scaffold.

Next, the dynamic mechanical behavior of the scaffolds under a constant strain with varying frequencies was observed. The viscoelastic properties are represented using the modulus values, including storage modulus (E') and loss modulus (E''). The storage modulus, considered to be the elastic part of the scaffolds, showed significantly higher values as MN content increased, ranging from 100 kPa (0% MNs) to 450 kPa (3% MNs) (**Fig. 4c**). The loss modulus values, thought to be the viscous part of the scaffolds, were also significantly higher with increasing MN content (from 60 kPa for 0% MNs to 150 kPa for 3% MNs) (**Fig. 4d**). The average values of the two moduli are summarized (**Fig. 4e**). In all compositions, the E' value was higher than the E" value, and the increase in E' was more noticeable in the MN-added scaffolds. The tan delta, determined from E"/E' and defined as the damping factor or loss parameter, was also plotted (**Fig. 4f**), and it showed that an increase in the MN content decreased the tan delta value substantially. The dynamic mechanical analysis results demonstrated that MNs incorporation enabled hybrid scaffolds to behave more elastically with substantial improvement in the storage modulus while also reducing damping. The incorporation of MNs within the hybrid scaffolds significantly improved the mechanical properties, as can be seen in the static and dynamic mechanical data, such as the elastic behaviors in dynamic load conditions and the resistance to deformation against a compressive load. These properties are considered to be effective for application of the magnetic hybrid scaffolds to hard tissue repair.

3.2. In Vitro Bioactivity and Stem Cell Responses

The bioactivity of the magnetic hybrid scaffolds was first examined via apatite-forming ability assay in SBF, which has been widely used to assess the acellular bone-bioactivity of biomaterials developed for bone [2,17,21,22]. Here the 1.5xSBF was used to accelerate the apatite-forming reaction and to thus shorten the observation period, as have also been proposed elsewhere. The SEM morphology of the scaffolds with different compositions after SBF-immersion for 7 days is shown in the representative images (**Fig. 5a**). All the scaffolds showed substantial mineralization with the whole surface covered throughout with layers of large apatite crystals. Crystal growth appeared to be more conspicuous, showing larger crystal colonies, in the 1%-MNs- and 2%-MNs-incorporated scaffolds than in the MNs-free and 3%-MNs-incorporated scaffolds. This was reasoned to be due to the fact that the MNs-dispersed in the hybrid matrix played some crucial role in the nucleation of apatite because the 3% MNs were distributed more densely in the matrix than the 1% and 2% MNs that were providing more nucleation sites and thus smaller crystal sizes [2,21]. The scaffold weight increased with respect to immersion time due to crystal formation (**Fig. 5b**). Weight increased almost linearly with time, and as early as 1 day the weight gain was ~10% and became ~60% after 14 days. Moreover, the degree of weight increase was comparable for all scaffolds except for that of the 3%-MNs-incorporated scaffold which showed a higher weight gain when compared to the others. In fact, the GS hybrid composition has been shown to have excellent apatite-forming ability [2,23,24], a fact which was also proven in this study, and the addition of MNs also influenced the apatite-forming behavior. It is considered that the incorporation of MNs at least preserves the apatite-forming ability, and even increases that ability, when incorporated at a large quantity (3%) by providing new nucleation sites for apatite crystals. The mineralized samples (3% MNs shown for representative sample) were further analyzed via XRD (**Fig. 5c**), which showed a sharp peak at $2\theta \sim 32^{o}$, characterizing the main peak of apatite. The FTIR spectrum of the scaffolds during SBF immersion revealed the development of chemical bands associated with apatite (phosphate bands). Based on the SBF test, the MNs-incorporated hybrid scaffolds were proven to have excellent apatite-forming ability, and thus to have effective bone-bioactivity for use as bone regenerative scaffolds.

We next sought to examine the cellular responses to the magnetic hybrid scaffolds. Rat MSCs were used to evaluate the performance of the scaffolds in cultivating stem cells and stimulating those stem

cells to engage in osteogenic differentiation, which is valuable information for bone tissue engineering of the scaffolds. Cell proliferation was measured via dsDNA assay after 7 and 14 days of culture time (**Fig. 6a)**. Cell proliferation on the scaffolds at 7 days was not substantially different, but became significantly different after 14 days. In particular, NMs-incorporated scaffolds showed higher cell proliferation than MNs-free scaffold (2% MNs > 3% MNs > 1% MNs > 0% MNs). The 2%-MNs scaffold showed almost twice that of the 0%-MNs scaffold. The SEM images showed the morphology of cells which were grown directly on the scaffolds (**Fig. 6b**). On all the hybrid scaffolds, the cells showed active cytoskeletal extensions with intimate contacts with the underlying substrates. The cells on the MNs scaffolds were more elongated, extending a number of highly extended filophodia processes, when compared to cells on the 0%-MNs scaffold. This was more noticeable particularly for the 2%-MNs and 3%-MNs scaffolds at 14 days, where significant cellular proliferation has been noticed. Thus, it is clear that the incorporation of MNs within the hybrid scaffolds stimulated cell proliferation and cytoskeletal processes which is an effective phenomenon of cells to enter into a next phase of osteogenesis. In fact, previous works have shown the importance of magnetic nanoparticles in increasing cell proliferation on different types of scaffolds. For instance, calcium phosphates impregnated with 20 nm magnetic nanoparticles showed a dose-dependent increase in the proliferation of osteoblasts [25,26]. Furthermore, magnetic nanoparticles incorporated within synthetic polymer scaffolds also increased the osteoblastic cell proliferation [27,28]. However, the exact reasons for this stimulatory role in cell proliferation have not yet been clarified.

We next sought to find the effects of MNs addition on osteogenic differentiation of rMSCs. First, ALP activity was determined to be the osteogenic marker of rMSCs that are committed to an osteogenic lineage. The 3%-MNs scaffold was tested as the representative sample for magnetic scaffolds against the MNs-free scaffold. Cells on both scaffolds were shown to have increased ALP levels during culture from 7 days to 14 days (**Fig. 7**). More importantly, when compared to the MNs-free scaffold, the 3%-MNs scaffold showed significantly higher ALP levels at 7 and 14 days, indicating that the magnetic scaffold provided better substrate conditions for the MSCs to undergo osteogenic differentiation. Previous reports have also shown that magnetic nanoparticles added to calcium phosphate ceramics considerably increased ALP activity relative to control ceramic samples [9,29].

Next we investigated cellular mineralization on the magnetic scaffolds. The mineralization stage is considered to be the final phase of osteogenesis, after sufficient bone matrix proteins have been secreted. The calcium deposited by the cells was quantified by using ARS staining. The images of ARS-stained and dye-eluted solutions of samples showed much clearer red signals on the 3%-MNs scaffold than on the MNs-free scaffold (**Fig. 8a**). The quantified calcium content measured at different culture periods (7 to 21 days) showed a significant increase with respect to time for both scaffolds, and a significantly higher calcium content on the 3%MNs scaffold was shown when compared to the MNs-free scaffold at all time periods. Cells cultured for 21 days on the magnetic scaffold were examined (**Fig. 8c**). The formation of some mineralized nodules was observed, and the morphology was readily noticeable when the cells were sufficiently differentiated and calcified [30].

In fact, the MNs-free GS hybrid scaffold used as a control herein is proven to be of bone-bioactive composition and is effective in driving rMSCs to engage in osteogenic lineage when cultured with osteogenic medium [31]. As such, ALP expression and calcium mineralization of cells on the MNs-free scaffold were shown to occur at sufficient levels in this study. However, the involvement of MNs improved further the cellular responses on the hybrid scaffolds in terms of proliferation and osteogenic development. Collectively, the MN incorporation into the GS hybrid scaffolds was proven to have great improvements in proliferation and osteogenic differentiation of MSCs. While some studies have also reported effective roles of magnetic nanoparticles in stimulating the proliferation and differentiation behaviors of osteoblasts when added to biomaterials, no exact mechanisms have yet been found [6,9,32,33].

Some possible explanations for such behaviors are as follows: first, the magnetic field generated due to the existence of MNs at the subcellular level would influence the cellular reactions. The cells sense the magnetism-induced microenvironment in a similar manner to mechanically-altered conditions in which the cells conform with changes in cell membrane receptors and the ion channels that signal the mechanotransduction processes, which lead to an alteration in cell cycles and differentiation of premature and/or stem cells [9,15,34]. In this manner, the investigation of the cellular responses to the magnetic materials under external magnetic fields might be an interesting study, which remains as future work. While very little has been carried out on this, one recent study has reported the positive effects of magnetic fields on the cell proliferation and osteogenic differentiation [9]. Secondly, the

possible dissolution of iron ions from the MNs, even when it happens at small quantities, could also affect the behavior of cells responsive to ionic products [9,34]. However, the exact discovery of these possible mechanisms, while worthwhile in the near future, is considered beyond the scope of this study.

4. Conclusions

MNs were incorporated effectively into the hybrid scaffolds of gelatin-siloxane during the sol-gel process. The MNs-incorporated scaffolds exhibited excellent magnetic properties, preserving the superparamagnetic behavior of native MNs. The incorporated MNs increased water uptake and swelling of the hybrid scaffolds while not accelerating hydrolytic degradation. The mechanical properties of the scaffolds, including the resistance to deformation and elasticity, were analyzed both statically and dynamically and were found to significantly improve with the addition of MNs, which are effective for use in bone-engineering scaffolds. The addition of MNs preserved the excellent apatite-forming ability of the hybrid scaffolds in simulated body fluid. Rat MSCs cultured on the magnetic scaffolds were shown to have significantly stimulated proliferation and osteogenic differentiation behavior, implying the effective role of incorporated MNs in providing substrate conditions for multiplication and osteogenesis of stem cells. Taken together, the MNs-incorporated GS hybrid scaffolds possess physico-chemical, mechanical, and biological properties which are effective for bone repair and tissue engineering.

Acknowledgement: This work was supported by the Priority Research Centers Program (grant#: 2009-0093829), National Research Foundation (NRF), Republic of Korea.

References

[1]R. A. Pérez, J. E. Won, J. C. Knowles and H. W. Kim, *Adv. Drug Deliv. Rev.*, 2013, **65**, 471–496.

[2]K. Dashnyam, R. A. Perez, E. J. Lee, Y. R. Yun, J. H. Jang, I. B. Wall and H. W. Kim, *J. Biomed. Mater. Res. A*, 2014, 102, 1859-1867.

[3] S. Chen, S. Chinnathambi, X. Shi, A. Osaka, Y. Zhu and N. Hanagata, *J. Mater. Chem*., 2012, **22**, 21885-21892.

[4]E. J. Lee, S. H. Jun, H. E. Kim, H. W. Kim, Y. H. Koh, J. H. Jang, *J. Mater. Sci. Mater. Med*, 2010, **21**, 207-214.

[5]E. J. Lee, S. H. Jun, H. E. Kim and Y. H. Koh, *J. Biomed. Mater. Res. A*, 2012, **100A**, 841-847

[6]N. Bock, A. Riminucci, C. Dionigi, A. Russo, A.Tampieri, E. Landi, et al, *Acta Biomater.*, 2010, **6**, 786–796.

[7]R. K.Singh, T. H. Kim, K. D. Patel, J. C. Knowles and H. W. Kim, *J. Biomed. Mater. Res. A,* 2012, **100**,1734–1742.

[8]J. Miyakoshi, Prog. Biophys. *Mol. Biol.*, 2005, **87**, 213–223.

[9] X. B. Zeng, H. Hu, L. Q. Xie, F. Lan, W. Jiang, Y. Wu, Z. W. Gu, *Int. J. Nanomed.,* 2012, **7,** 3365-3378.

[10]R. K. singh, K. P. Patel, J. H. Lee, E. J. Lee, J. H. Kim, T. H. Kim and H. W. Kim, *PLoS One*, 2014, **9**, e91584.

[11]L. Dini and L. Abbro, *Micron.*, 2005, **36**, 195–217.

[12]L. Potenza, L. Ubaldi, R. De Sanctis, R. De Bellis, L. Cucchiarini and M. Dachà, *Mutat. Res.*, 2004, **561**, 53–62.

[13]K. Shimizu, A. Ito and H. Honda, *J. Biomed. Mater. Res. B Appl. Biomater*., 2006, **77**, 265–272.

[14]C. F. Adams,M. R. Pickard and D. M. Chari, *Nanomedicine*, 2013, **9**, 737–741.

[15]J. J. Kim, R. K. Singh, S. J. Seo, T. H. Kim, J. H. Kim, E. J. Lee and H. W. Kim, *RSC Adv.*, 2014, **4**, 17325-17336.

[16]L. H. Reddy, J. L. Arias, J. Nicolas and P. Couvreur, *Chem. Rev.*, 2012, **112**, 5818–5878.

[17]J. H. Kim, H. J. Moon, T.H. Kim, J.M. Jo, S.H. Yang, D. Naskar, S.C. Kundu, W. Chrzanowski, H. W. Kim, *J. Tissue Eng.*, 2012, **4**, 2014731413517705.

[18]R. A. Perez, M. Kim, T. H. Kim, J. H. Kim, J. H. Lee, J. H. Park, J. C. Knowles and H. W. Kim, *Tissue Eng. Part A*, 2014, **20**, 103-114.

[19]J. E. Won, A. El-Fiqi, S. H Jegal, C. M. Han, E. J. Lee, J. C. Knowles, H. W. Kim, *J. Biomater. Appl.,* 2014, **28**, 1213-1225.

[20]B. B. Doyle, E. G. Bendit and E. R. Blout, *Biopolymers*, 1975, **14**, 937-957.

[21]L. Ren, K. Tsuru, S. Hayakawa and A. Osaka, *Biomaterials*, 2002, **23**, 4765–4773.

[22]S. H. Shin, D. Purevdorj, O. Castano, J. A. Planell, H. W. Kim, *J Tissue Eng*, 2012, **3**, 2014731412443530.

[23]B. H. Yoon, H. E. Kim and H. W. Kim, *J. Mater. Sci. Mater. Med.*, 2008, **19**, 2287–2292.

[24]M. Mozafari, F. Moztarzadeh, M. Rabiee, M. Azami, S. Maleknia, M. Tahriri, Z. Moztarzadeh and N. Nezafati, *Ceram. Int.*, 2010, **36**, 2431–2439.

[25]R. A. Pareta, E. Taylor T. J. Webster, *Nanotechnology*, 2008, **19**, 265101.

[26]S. Kwon, R. K. Singh, R. A. Perez, E. A. Abou Neel, H. W. Kim and W. Chrzanowski, *J. Tissue Eng.*, 2013, **4**, 2041731413503357.

[27]Y. Zhao and Y. Guo, *Int. J. Nanomed.* 2012, **5**, 593–602.

[28]C. Heinemann, S. Heinemann, A. Bernhardt, H. Worch and T. Hanke, *Biomacromolecules*, 2008, **9**, 2913– 2920.

[29]Y. Wu, W. Jiang, X. Wen, B. He, X. Zeng, G. Wang and Z. Gu, *Biomed. Mater.*, 2010, **5**, 15001.

[30]M. T. Rodrigues, A. Martins, I. R. Dias, C. A. Viegas, N. M. Neves, M. E. Gomes and R. L. Reis, *J. Tiss. Eng. Reg. Med.*, 2012, **6**, 24-30.

[31]R. A. Perez, H. W. Kim and M. P. Ginebra, *J. Tissue Eng.*, 2012, **3**, 2041731412439555.

[32]J. Miyakoshi, *Prog. Biophys. Mol. Biol.*, 2005, **87**, 213–23.

[33]C. Fanelli, S. Coppola, R. Barone, C. Colussi, G. Gualandi, P. Volpe and L. Ghibelli, *FASEB J.*, 1999, **13**, 95–102.

[34]C. C. Berry and A. S. G. Curtis, *J. phys. D Appl. Phys.*, 2003, **36**,198.

Figure Caption

Figure 1. (a) SEM morphology of the bioactive gelatin-siloxane hybrid scaffolds with the incorporation of varying contents (1, 2, and 3%) of MNs. (b) The TEM image of the 3%-MNs scaffolds, shown as a representative sample, revealed homogeneous distribution of the nanoparticles (black dots). (c) XRD pattern of the scaffolds. The asterisk symbol represents the magnetite peaks. (d) FT-IR spectrum of the scaffolds, showing chemical bond structure. Spectrum of MNs also included for reference.

Figure 2. Magnetic properties of the hybrid scaffolds. (a) Minimum distance at which the scaffolds are attracted by a static magnet. (b,c) Measurement of magnetization behaviors by SQUID, shown at a large and small magnetic field range. (d) Saturation magnetization, Ms, measured from the magnetization curves.

Figure 3. (a) Ethanol uptake level, meant to be the porosity of the hybrid scaffolds. (b) Water uptake capacity with time, (c) swelling degree of the hybrid scaffolds at 4 h after soaking in distilled water. (d) Degradation of the hybrid scaffolds in PBS for up to 28 days.

Figure 4. Mechanical properties of the hybrid scaffolds. (a) Strain recorded with respect to time on applying a constant static compressive load, and (b) strain determined at 300 s. (c-f) Dynamic mechanical analysis of scaffolds: (c) Storage modulus, E', (d) loss modulus E", (e) average modulus values summarized, and (f) tan delta (δ) .

Figure 5. In vitro apatite-forming ability of the hybrid scaffolds during immersion in 1.5xSBF for different periods. (a) SEM image of scaffolds after 7 days of immersion, and (b) weight change with respect to immersion time. (c) XRD and (d) FT-IR of the 3%-MNs scaffold during immersion.

Figure 6. In vitro cell behaviors on the hybrid scaffolds. (a) Cell proliferation measured by dsDNA quantification. Cell proliferation at 14 days was significantly higher than that at 7 days for all groups (*$p < 0.05$). A significant difference was shown when comparing between groups at 14 days (marked by the symbols '*a,b,c,d*'; $p < 0.05$). (b) Representative SEM image of cells at 7 and 14 days.

Figure 7. ALP activity of cells at days 7 and 14, represented after being normalized to DNA content. A significant difference was noticed between the groups (*$p < 0.05$) at each period, and between periods ($^{\#}p < 0.05$) at each group.

Figure 8. Cellular mineralization behavior, examined by ARS staining. (a) Image showing ARS stained samples (above) and eluted product solutions (below) at different culture periods for 0%-MNs and 3%-MNs scaffolds. (b) Calcium content assayed by optical density, and (c) SEM cell images showing the appearance of cellular calcification at day 21 (3%-MNs scaffold). A significant difference was noticed between the groups (*$p < 0.05$) at day 21.

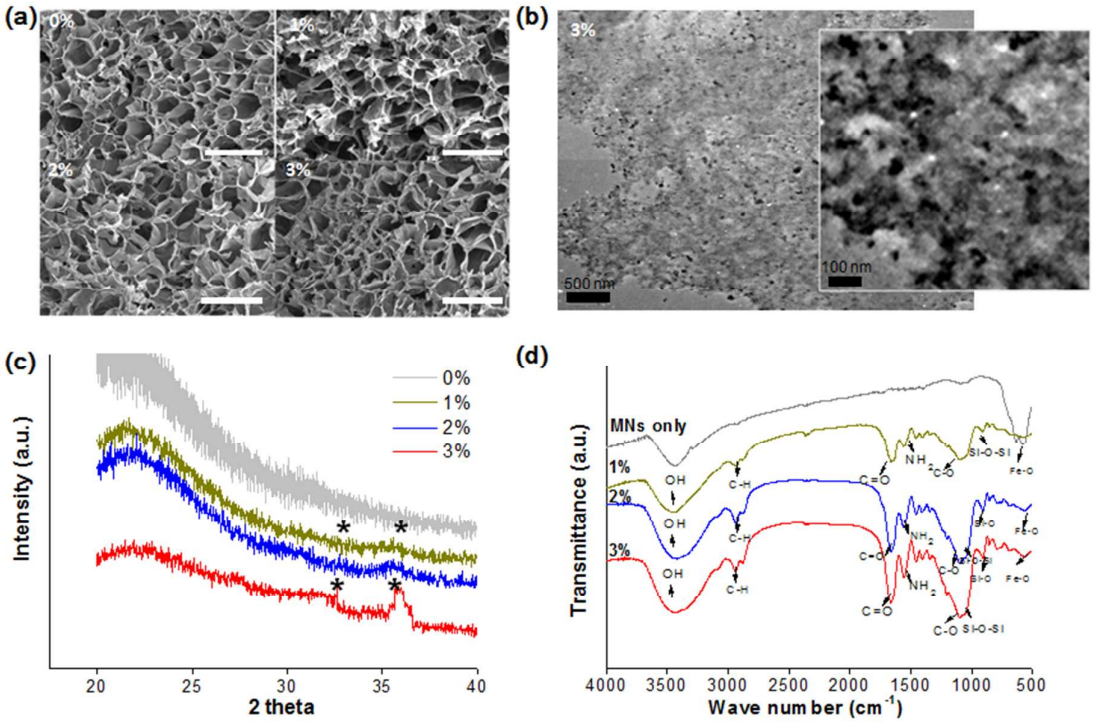

Fig. 1

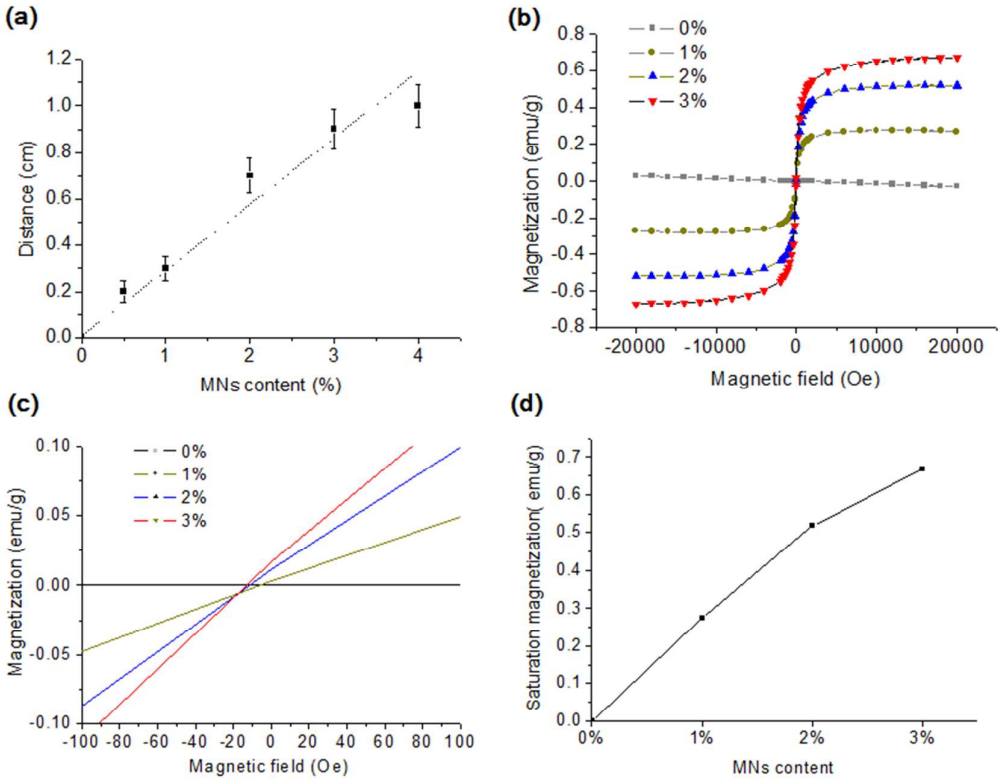

Fig. 2

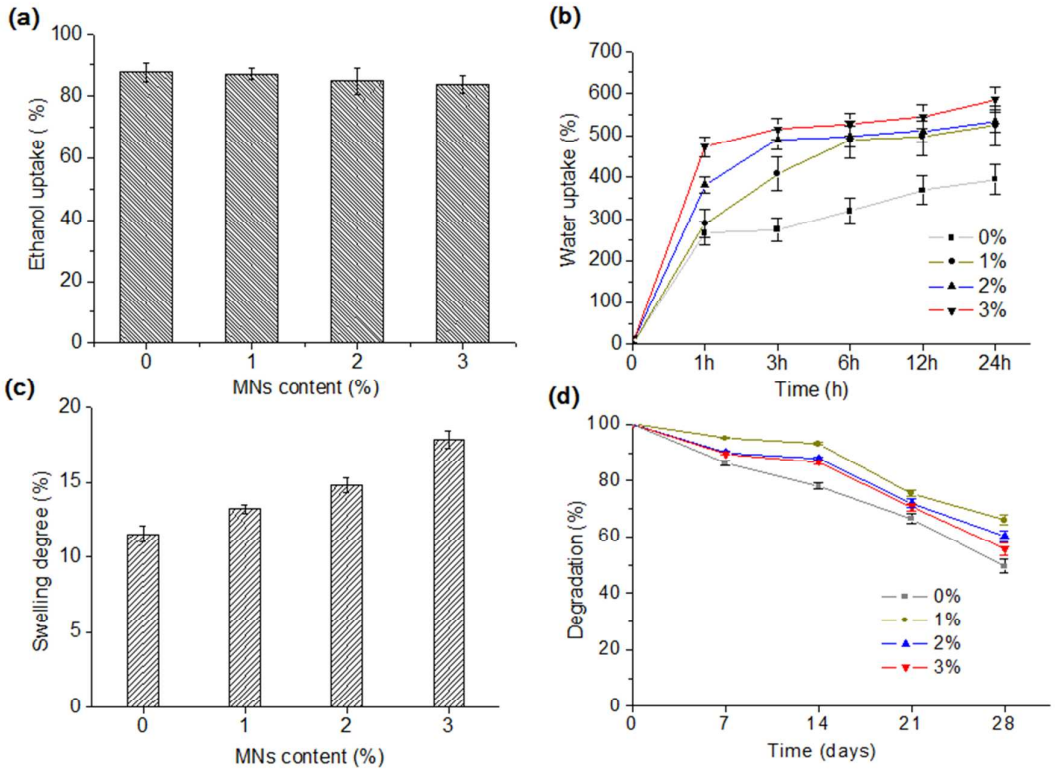

Fig. 3

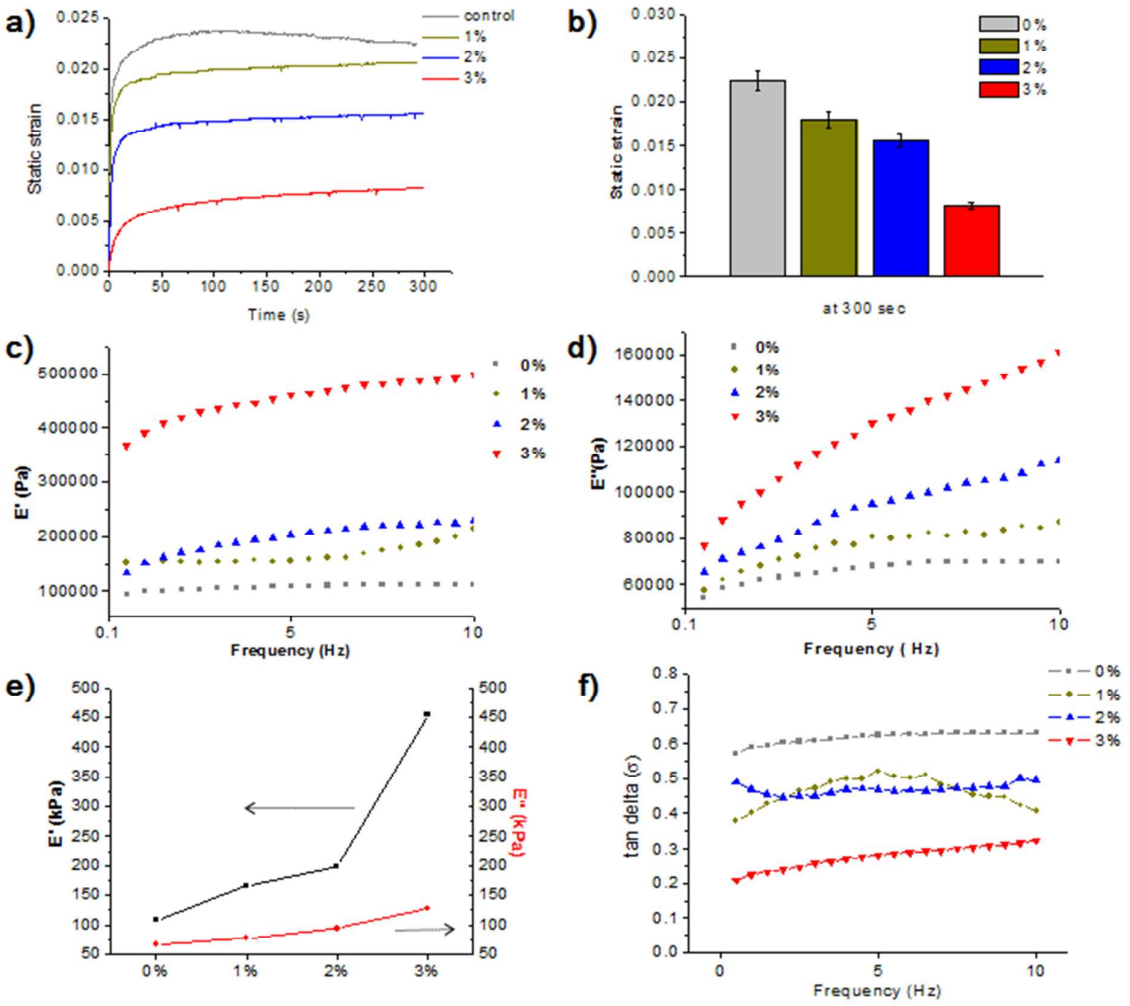

Fig. 4

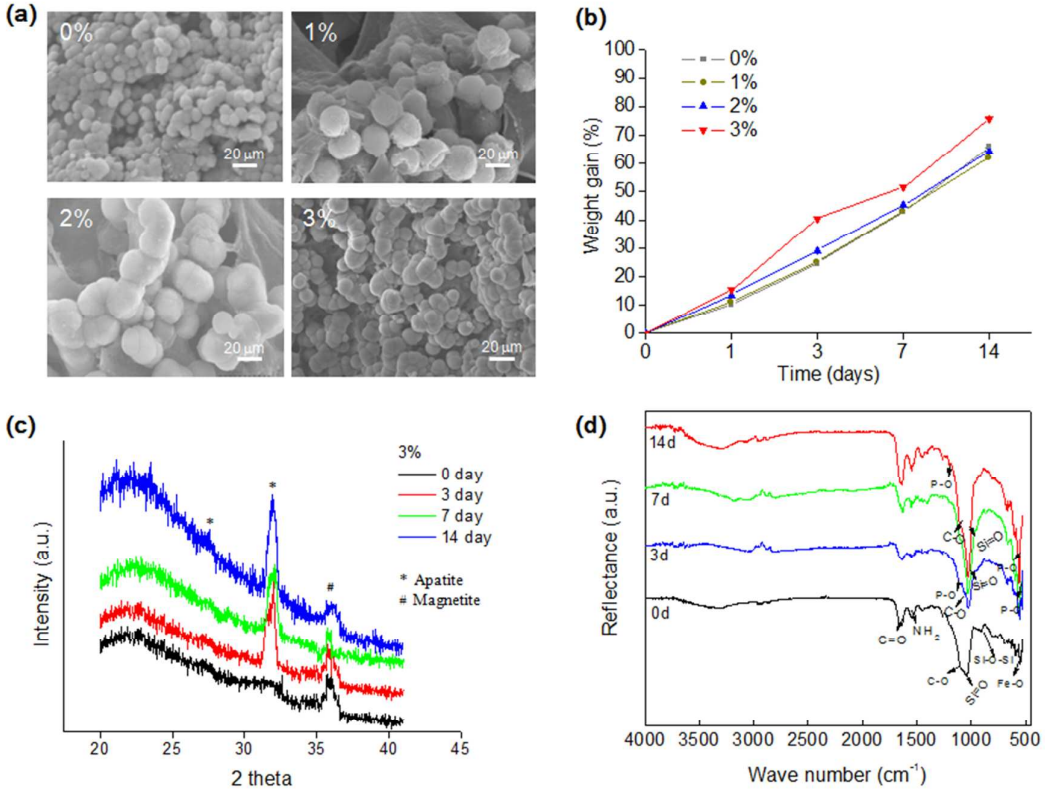

Fig. 5

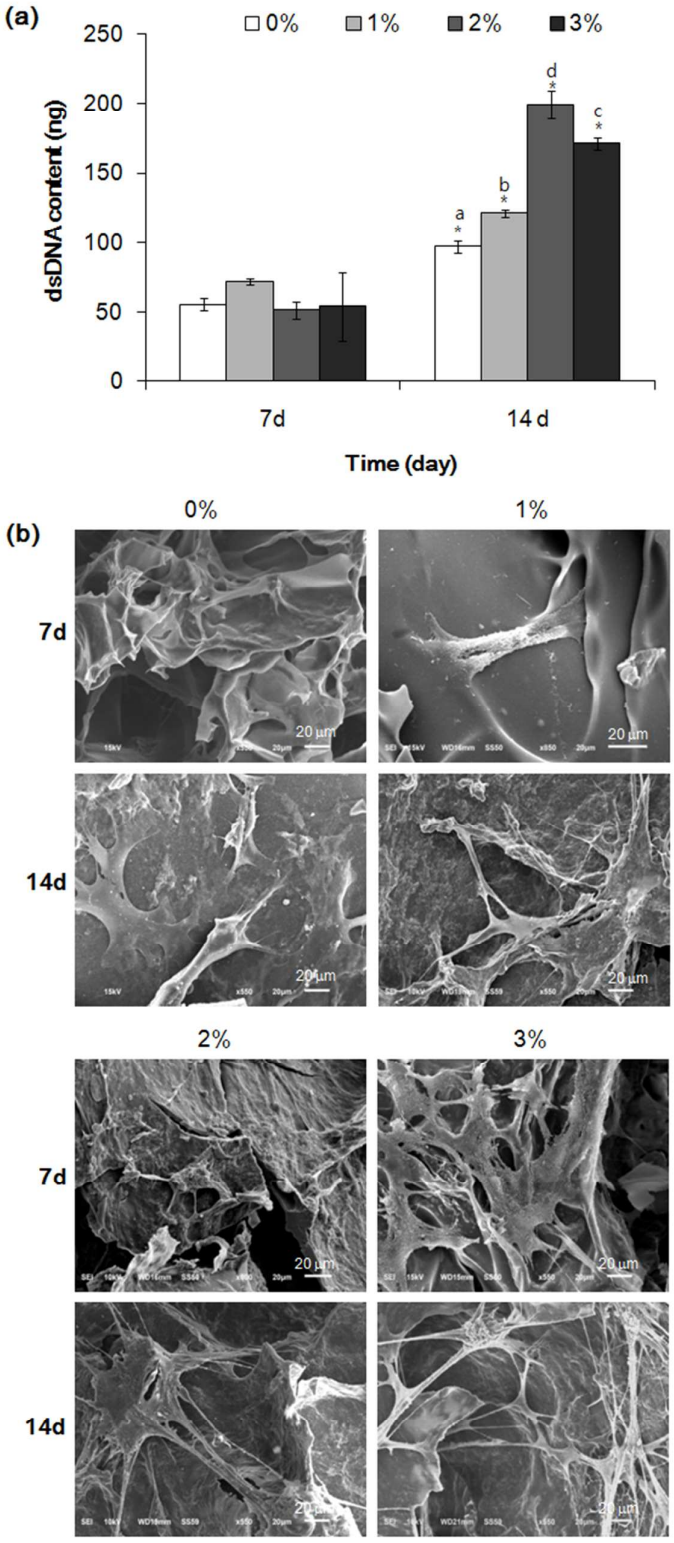

Fig. 6

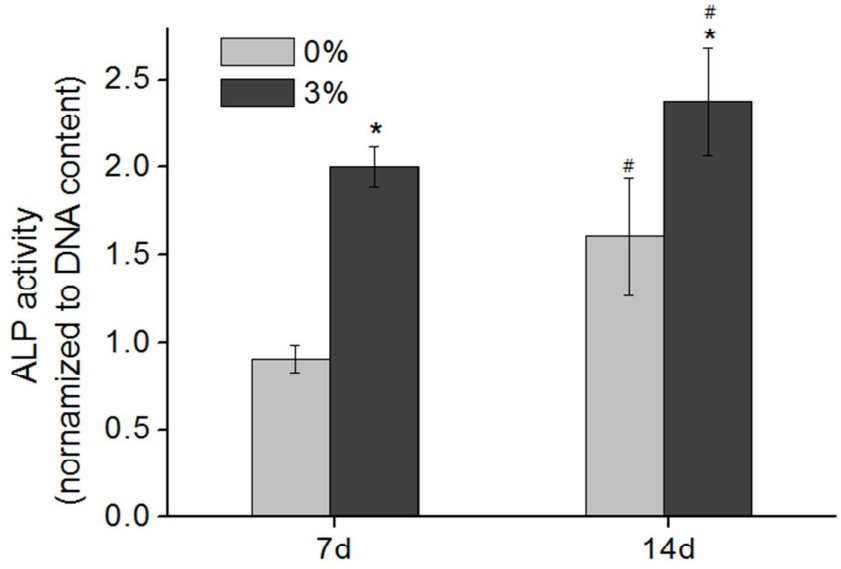

Fig. 7

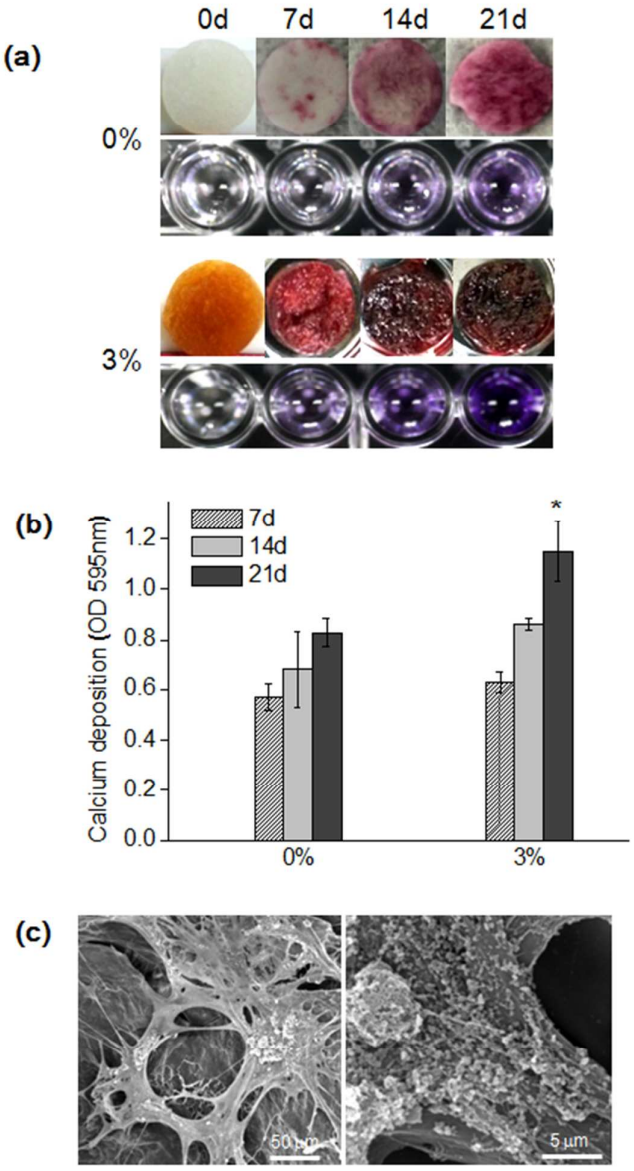

Fig. 8

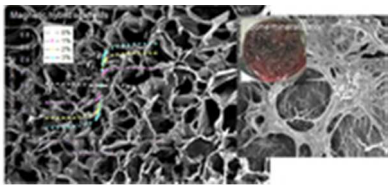

Hybrid magnetic scaffolds of silica-gelatin-MNPs newly developed to have excellent physicochemical, mechanical and biological properties that are effective for bone tissue engineering
16x7mm (300 x 300 DPI)